Acta Cryst. (1979). A**35**, 901–911

The Oscillation Method for Crystals with Very Large Unit Cells

BY F. K. WINKLER,* C. E. SCHUTT† AND S. C. HARRISON

Gibbs Laboratory, Harvard University, 12 Oxford Street, Cambridge, Massachusetts 02138, USA

(*Received* 20 *February* 1979; *accepted* 17 *May* 1979)

Abstract

The processing of data collected by oscillation photography from crystals with very large unit cells (average cell constant $\gtrsim 250$ Å) requires important modifications of standard methods. In particular, it is often necessary to correct partially recorded intensities to their fully recorded equivalents. A procedure is described for accurate determination of relevant parameters (crystal setting, cell constants). It relies on the redundancy present in most data-collection strategies, which yields fully recorded, symmetry-related counterparts of a number of partially recorded reflections. A detailed description of one example (tomato bushy stunt virus) is presented, with complete intensity statistics.

Introduction

The oscillation method (Arndt & Wonacott, 1977) is now generally accepted as the most efficient means for photographic data collection from crystals with unit-cell dimensions greater than about 100 Å. For very large unit cells (average dimensions greater than about 250 Å), the usual method must be modified to realize its full efficiency – in particular, to cope with situations where only one good photograph, instead of a series of contiguous ones, can be taken within the lifetime of a crystal. Essentially, the resulting 'one crystal–one photograph' condition requires a different treatment of partially recorded reflections. This paper describes general aspects of the new procedure and gives a detailed account of its application to data collection from crystalline tomato bushy stunt virus (TBSV: space group $I23$, $a = 383{\cdot}2$ Å) to 2·9 Å resolution.

I. The problem of partially recorded reflections

The angular range of an oscillation photograph is generally chosen by the criterion that no two reciprocal lattice points at a desired resolution limit have overlapping spots on the film. The allowable range per photograph is limited by the magnitudes of the cell dimensions, the resolution limit, and the angle over which a Bragg reflection will diffract. For example, with TBSV crystals, which have an average reflecting range (determined largely by the Franks-camera beam cross-fire) of about 10′ of arc, the allowable oscillation range at 2·9 Å resolution is only 30′. In some other cases, where larger ranges would be permitted by geometrical criteria, the oscillation is restricted in practice by accumulation of background exposure. An unavoidable consequence of a finite reflecting range is that the intensity at reciprocal lattice points near the ends of the oscillation range is recorded only partially on the film. If these partially recorded reflections cannot be used, the efficiency of the recording process is lowered. In the standard procedure using contiguous photographs, intensities of complementary parts of a reflection, split between two successive photographs, are combined to give the fully recorded equivalent. For large unit-cell volumes, exposure times required for a good average signal-to-noise ratio on the film approach the lifetime of the crystal. In the limit, only one photograph can be obtained and partial spot addition is impossible.

There are two ways of proceeding when partial spot addition cannot be used. If their number is relatively small, partial spots can simply be discarded. In high-resolution data collection from large unit cells, however, a majority of spots can fall in this category (around 75% for TBSV with a 30′ rotation range), and the only way of avoiding the inefficiency of discarding them is to correct each partial to its fully recorded equivalent. Accurate correction to fully recorded equivalents depends critically on crystal-setting and unit-cell parameters, since there is no margin of safety afforded by taking an artificially higher value for the reflecting range, as in cases where partial spots are added or discarded. Moreover, calculation of recorded fractions demands knowledge not only of the width of the reflecting curve but also of its normalized profile. Thus, the need to know the shape and exact width for the normalized rocking curve is a new feature of efficient data collection in the one crystal–one photograph situation.

* Present address: EMBL, Postfach 10.2209, 69 Heidelberg, Federal Republic of Germany.

† Present address: MRC Laboratory of Molecular Biology, Hills Road, Cambridge CB2 2OH, England.

0567-7394/79/060901-11$01.00

We describe in the sections below a method for correcting partially recorded reflections to their fully recorded equivalents. The method relies on redundancy in the data-collection scheme, such that a number of reflections partially recorded on a given photograph have equivalent, fully recorded reflections on the same or another photograph. The ratio of any such pair of intensity measurements is an 'observed' recorded fraction, each of which is a measure of the crystal-setting, unit-cell, and rocking-curve parameters. If these parameters are sufficiently over-determined (that is, if the number of partials having fully recorded counterparts elsewhere in the data set is sufficiently great), a straightforward, least-squares refinement procedure can be adopted. It yields far more accurate values for the required parameters than are obtained in the usual refinement based on visually observed partial spots. The approach can be applied in principle to any oscillation photograph, but since a suitably over-determined refinement implies large numbers of partially recorded reflections on a single film, the method is restricted in practice to relatively large unit cells.

II. Crystal orientation geometry

The notation followed here to describe crystal orientation is that used by Crawford (1977) in the 'Harvard system' (Arndt & Wonacott, 1977, p. 140). The laboratory frame, centered at the origin of reciprocal space, is defined such that the X axis is parallel to the incident beam, the Z axis parallel to the camera spindle and the Y axis orthogonal to these two. From one of six possible reference orientations, defined by which real axis is along Z and which reciprocal axis along X, the reciprocal lattice is brought to a required orientation by applying in turn the three rotations ψ, ω, and φ around axes X, Y and Z, respectively (Fig. 1). Note that coincidence of oscillation angle and setting angle φ implies zero inclination. The equations developed below would require modification for other inclination angles. The laboratory coordinates of reflection i at setting (ψ,ω,φ) are then obtained by applying two successive transformations represented by the matrices A and B:

$$\begin{pmatrix} x_i \\ y_i \\ z_i \end{pmatrix} = BA \begin{pmatrix} h_i \\ k_i \\ l_i \end{pmatrix}. \qquad \text{(II.1)}$$

The two matrices are:

$$A = \begin{pmatrix} a^* & b^* \cos\gamma^* & c^* \cos\beta^* \\ 0 & b^* \sin\gamma^* & c^*(\cos\alpha^* - \cos\beta^* \cos\gamma^*)/\sin\gamma^* \\ 0 & 0 & c^* \cos(c^*, c) \end{pmatrix};$$

where

$$\cos(c^*, c) = (1 + 2\cos\alpha^* \cos\beta^* \cos\gamma^* - \cos^2\alpha^* - \cos^2\beta^* - \cos^2\gamma^*)^{1/2}/\sin\gamma^*.$$

A orthogonalizes the reciprocal lattice, and as given above corresponds to the reference orientation with a^* along X and c along Z.

At the time an oscillation photograph is taken we have only approximate values for the setting angles, which we call the *nominal setting angles* ψ_0, ω_0 and φ_0^t. Superscript t refers to a specific value of the oscillation angle φ; for example, $t = b$ refers to the beginning, $t = e$ to the end, and $t = m$ to the middle of the oscillation range, $\Delta\varphi = \varphi^e - \varphi^b$. More accurate values for these angles can be obtained from the orientation information present on each photograph in the form of partially recorded reflections (§ IV) or in the positions of fully recorded reflections (Arndt & Wonacott, 1977, Chapter 8). This information is used in a least-squares refinement to determine the misorientation of the crystal

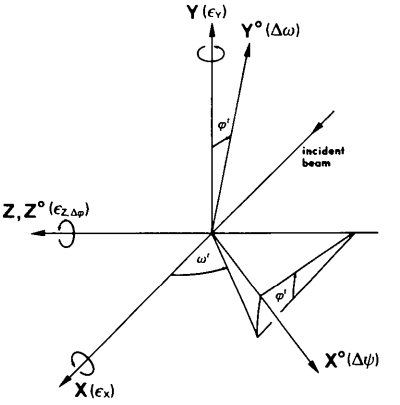

Fig. 1. Definition of the laboratory coordinate system X, Y, Z and of the rotations ψ, ω, φ. Positive rotations are defined as anticlockwise when looking down the rotation axis. The three rotations ψ, ω, and φ applied in turn around these axes do not correspond to an Eulerian set of angles, since the rotation axes are defined in the fixed laboratory space and not in the rotated reciprocal space. X^0 is the position of an axis, initially coincident with X, after application of the rotations ω and φ; Y^0, the position of an axis initially coincident with Y, after application of the rotation φ. At setting t ($\varphi = \varphi^t$), a correction $\Delta\psi$ corresponds to a rotation about X^0; likewise, a correction $\Delta\omega$ to a rotation about Y^0. A correction $\Delta\varphi$ is always taken about the oscillation axis; Z and Z^0 are therefore drawn coincident. Obviously, axes for the three corrections are not orthogonal. This leads to difficulties only when ω approaches $\pi/2$ (some elements of II.2 become very large), and this case must be avoided by choosing another initial reference orientation. The corrections $\Delta\psi$, $\Delta\omega$, $\Delta\varphi$ are related to laboratory-frame angular adjustments by (II.2).

$$B = \begin{pmatrix} \cos\omega\cos\varphi & \sin\psi\sin\omega\cos\varphi - \cos\psi\sin\varphi & \cos\psi\sin\omega\cos\varphi + \sin\psi\sin\varphi \\ \cos\omega\sin\varphi & \sin\psi\sin\omega\sin\varphi + \cos\psi\cos\varphi & \cos\psi\sin\omega\sin\varphi - \sin\psi\cos\varphi \\ -\sin\omega & \sin\psi\cos\omega & \cos\psi\cos\omega \end{pmatrix};$$

from its nominal setting. The *misorientation angles*, ε_x^t, ε_y^t, and ε_z^t, are small rotations around laboratory-frame axes X, Y and Z respectively, *at setting t*, and are equivalent to ψ_X, ψ_Y, and ψ_Z in Arndt & Wonacott (1977). As shown in Fig. 1, the corrections to the setting angles, $\Delta\psi$, $\Delta\omega$ and $\Delta\varphi$, can be considered as rotations about X^0, Y^0, Z^0, and only in the special case $\omega = \varphi = 0$ are the rotation axes of ψ and ε_x or of ω and ε_y identical. If only small corrections have to be applied to the setting angles, they are well approximated by the transformation

$$\begin{pmatrix}\Delta\psi\\ \Delta\omega\\ \Delta\varphi\end{pmatrix} = \begin{pmatrix}\cos\varphi^t/\cos\omega & \sin\varphi^t/\cos\omega & 0\\ -\sin\varphi^t & \cos\varphi^t & 0\\ \cos\varphi^t\tan\omega & \sin\varphi^t\tan\omega & 1\end{pmatrix}\begin{pmatrix}\varepsilon_x^t\\ \varepsilon_y^t\\ \varepsilon_z^t\end{pmatrix}. \quad \text{(II.2)}$$

III. Choice of rocking curve model

The picture of a reciprocal lattice point crossing the Ewald sphere represents an idealized experimental situation, since real crystals diffract real X-ray beams over finite angular ranges. The construction can be adapted to this situation by replacing each reciprocal lattice point with a volume element, while retaining a geometric Ewald sphere. The boundaries and intensity distribution of this volume element are determined by four experimental factors: crystal morphology and size, crystal mosaicity, spectral dispersion, and X-ray beam geometry (Alexander & Smith, 1962). The rocking curve is the profile of diffracted intensity, integrated over the area of a spot on the detector, as a function of the angle of crystal rotation. In reciprocal space, each point of this profile corresponds to the passage of an infinitesimal section of the volume element through the Ewald sphere. Over the small area traversed by the volume element of a reflection, this sphere is well represented by a plane. The one-dimensional rocking curve can therefore be generated by projecting, at each angle of rotation, the contents of the corresponding infinitesimal section onto the normal to the Ewald sphere. A partially recorded reflection will have part of its volume inside and part outside the Ewald sphere at either φ^b or φ^e, and its recorded fraction, corresponding to one of these parts, depends only on the final position and not on the actual path of the volume element during rotation. In order to obtain a one-dimensional profile it is necessary to map the contents of the volume element, described above, onto an appropriate arc that intersects the Ewald sphere. Note that the arc of actual rotation would not be a very convenient choice, since the profile width would vary with the angular position of the reflection. The obvious choice is the β arc of each reflection, defined as the arc that describes the shortest angular separation of reciprocal lattice point P_i from the Ewald sphere, and illustrated in Fig. 2. The β axes all lie in the central plane perpendicular to the X-ray beam. The convenience or advantage of this choice is best illustrated by an example. Let us assume that the beam cross-fire is rotationally invariant, that crystal mosaicity is negligible or isotropic, and that the radiation is monochromatic. Under these conditions, not far from reality in TBSV data collection, the rocking curve, when defined on the individual β arcs, is the same for all reflections.

Using the angular variable β, we define the rocking curve as follows. Let β_i be the position of the center of the profile on the β arc of reflection i, which intersects the Ewald sphere at the Bragg angle θ_i. Assuming further a symmetric profile, the recorded fraction P_{cal}^i can be expressed as:

$$P_{\text{cal}}^i = 0{\cdot}5\{1 \pm f[(\beta_i - \theta_i)/\gamma_i]\} = 0{\cdot}5[1 \pm f(b_i)], \quad \text{(III.1)}$$

where $f(b_i)$ is an as yet unspecified function whose value is restricted to the range 0 to 1. The plus or minus

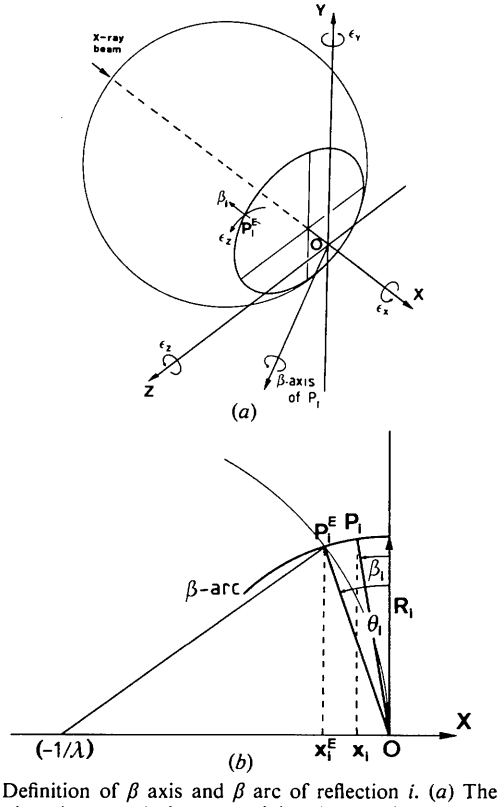

Fig. 2. Definition of β axis and β arc of reflection i. (*a*) The axis normal to the central plane containing the X axis and the lattice point P_i is defined as the β axis of P_i. We denote as P_i^E the position of P_i when it happens to lie on the Ewald sphere. Note that rotation about X causes P_i^E to trace out a circle on the surface of the Ewald sphere and that rotation of P_i about its β axis generates an arc (β_i) perpendicular to this circle. A positive rotation about the β axis is defined as producing a negative component on the X axis. (*b*) View along β axis of P_i. At P_i^E, β_i^E is equal to the Bragg angle θ_i. x_i is the x coordinate of P_i, and x_i^E, that of P_i^E.

sign indicates whether the reflection is more or less than half recorded. The function $f(b_i)$ gives the fractional intensity integrated on the rocking curve between β_i and θ_i. The half width of the profile of reflection i, γ_i, may itself be a function of various parameters γ_r and of certain geometric variables. For profiles of finite width, b_i is restricted to the range -1 to 1.

An important assumption in this approach is that a one-dimensional, normalized profile, specified by only a few parameters, is sufficient to describe the fractional build-up of intensity for all reflections as they pass through the Ewald sphere. A similar assumption is made in methods using learned profiles to obtain improved integrated intensities (Diamond, 1969; Grant & Gabe, 1978). In our work we used simple one-parameter curves whose integrals exist in analytical form. The need for possible improvements or extensions was examined later by looking for systematic discrepancies between calculated and observed fractions recorded. Two functions, both with a finite width 2γ, were tried as rocking-curve profiles:

(1) a step function, yielding for the integral f

$$f(b_i) = |b_i|; \tag{III.2}$$

(2) a cosine half wave, yielding for the integral f

$$f(b_i) = \left|\sin\left(\frac{\pi}{2} b_i\right)\right| = \sin\frac{\pi}{2}|b_i|. \tag{III.3}$$

Two extensions of these one-parameter functions were also considered.

(1) To model anisotropy of crystal mosaicity or beam crossfire, the half-reflecting range was allowed to vary continuously from γ_y to γ_z, in going from meridional ($\alpha = 0$) to equatorial ($\alpha = \pi/2$) reflections:

$$\gamma_i(\alpha_i) = [(\gamma_y \cos\alpha_i)^2 + (\gamma_z \sin\alpha_i)^2]^{1/2}, \tag{III.4}$$

The need for such a modification should become apparent if the differences between calculated and observed fractions are analyzed as a function of the angular position, α_i, of the reflections. For example, if the calculated fractions for the class of partial reflections less than half recorded near the meridian are systematically underestimated, while the same class is overestimated for reflections near the equator, then γ_y should be made larger than γ_z. This will be confirmed if the classes of reflections more than half recorded are found to have the opposite systematic trends.

(2) To take account of the increase of the reflecting range with resolution due to spectral dispersion, γ_i can be expressed as:

$$\gamma_i = \gamma_0 + \gamma_1 \tan\theta_i, \tag{III.5}$$

where

$$\gamma_1 = \Delta\lambda/2\lambda.$$

For the case of the Cu $K\alpha$ doublet $\Delta\lambda/\lambda$ is 0·0026. These two modifications are easily combined to yield a three-parameter rocking curve. For TBSV data only the second one was needed (§ V) and no more detailed models were tried in practice.

IV. Refinement of crystal-setting, unit-cell and rocking parameters

We assume a reference data set, constructed, for example, from fully recorded reflections scaled together from a number of photographs (for details, see § V). For any photograph, the observations used in parameter refinement are those reflections also present in the reference data set. It is important that there is a sufficient number of observations, with a uniform distribution over the area of the film. The reflections in the reference data set (usually an incomplete data set) should therefore be uniformly distributed in space.

Given n observations, the quantity minimized in the least-squares refinement is defined as

$$\Phi = \sum_{i=1} w_i(\Delta I_i)^2, \tag{IV.1}$$

where

$$\Delta I_i = I_p^i - P_{\text{cal}}^i I_R^i \tag{IV.2}$$

and

$$1/w_i = \sigma^2(\Delta I_i) = \sigma^2(I_P^i) + (P_{\text{cal}}^i)^2\,\sigma^2(I_R^i). \tag{IV.3}$$

I_P^i, $\sigma(I_P^i)$ are the intensity and estimated standard deviation (see § V) of the partially recorded reflection i, and I_R^i, $\sigma(I_R^i)$ are the intensity and e.s.d. of this reflection in the reference data set.

For obtaining the normal equations, which give the shifts Δp_j of the m parameters to be refined, Φ is linearized as usual by expansion in a Taylor series with elimination of higher terms. These m equations ($n > m$) can be written

$$-\sum_{i=1}^{n} w_i \Delta I_i \left(\frac{\partial \Delta I_i}{\partial p_j}\right)_0 = \sum_{i=1}^{n} w_i \left(\frac{\partial \Delta I_i}{\partial p_j}\right)_0 \sum_{k=1}^{m} \left(\frac{\partial \Delta I_i}{\partial p_k}\right) \Delta p_k, j = 1, \ldots, m, \tag{IV.4}$$

or after substituting ΔI_i by (IV.2), as

$$\sum_{i=1}^{n} w_j \Delta I_i I_R^i \left(\frac{\partial P_{\text{cal}}^i}{\partial p_j}\right)_0 = \sum_{i=1}^{n} w_i (I_R^i)^2 \left(\frac{\partial P_{\text{cal}}^i}{\partial p_j}\right)_0 \sum_{k=1}^{m} \left(\frac{\partial P_{\text{cal}}^i}{\partial p_k}\right)_0 \Delta p_k, j = 1, \ldots, m. \tag{IV.5}$$

The '0' subscript indicates evaluation of the partial derivatives for current values of the parameters. This evaluation requires some comment.

(1) *Rocking curve parameters, γ_r*

These derivatives depend on the functional form of $f(b_i)$ and of the particular parametrization of the rocking curve width. In a general way they are given as

$$\frac{\partial P^i_{\rm cal}}{\partial \gamma_r} = \pm \frac{1}{2} \frac{\partial f(b_i)}{\partial \gamma_i} \frac{\partial \gamma_i}{\partial \gamma_r}. \qquad \text{(IV.6)}$$

(2) *Crystal setting and unit-cell parameters*

The discussion in the previous section has shown that the width of the rocking curve itself may vary – for example, with the angular position of a spot on the film or with resolution (III.4 and III.5). However, this dependence can be neglected for calculation of partial derivatives, since the small shifts expected for orientation and unit-cell parameters have almost no effect on the width of the rocking curve of a particular reflection. For the case of the symmetrical profile where

$$P^i_{\rm cal} = 0{\cdot}5 \left[1 \pm f\left(\left|\frac{\Delta\beta_i}{\gamma_i}\right|\right)\right], \text{ with } \Delta\beta_i = \beta_i - \theta_i,$$

the derivatives with respect to these parameters can therefore be written as

$$\frac{\partial P^i_{\rm cal}}{\partial p_j} = \pm \frac{1}{2} \frac{\partial f}{\partial \Delta\beta_i} \frac{\partial \Delta\beta_i}{\partial p_j} \operatorname{sign}(\Delta\beta_i). \qquad \text{(IV.7)}$$

The partial derivatives $\partial\Delta\beta_i/\partial p_j$ describe the dependence of the angular distance, $\Delta\beta_i$, of reciprocal lattice point i from the Ewald sphere on crystal orientation and unit-cell parameters. Since the Bragg angle θ_i does not depend on the setting angles, the derivatives with respect to orientation parameters reduce to $\partial\beta_i/\partial\varepsilon_j$. For reflections close to the sphere, $\beta_i \simeq \theta_i$ (the Bragg angle), and these derivatives are:

$$\partial\beta/\partial\varepsilon_x = 0,$$
$$\partial\beta/\partial\varepsilon_y = -z_i/R_i \cos\theta_i,$$
$$\partial\beta/\partial\varepsilon_z = y_i/R_i \cos\theta_i,$$

where $R_i(=d_i^*)$ is the length of the reciprocal-lattice vector to the reflection i. As rotation around the beam direction X has no component on the β arc of reflection i, the first derivative must be zero. The other two are easily verified by considering the special cases of meridional and equatorial reflections. For the former, a rotation around the β axis is equivalent to a rotation around Z (ε_z), and the derivatives have to be ± 1 and 0 respectively, corresponding to $|y_i| = R_i \cos\theta_i$ and $z_i = 0$ for such reflections. To evaluate the derivatives of $\Delta\beta_i$ with respect to unit-cell parameters, p^c_j, we use the fact (see Fig. 2) that

$$\sin\beta_i = -x_i/R_i \quad \text{and} \quad \sin\theta_i = -x_i^E/R_i.$$

The derivatives $\dfrac{\partial\Delta\beta_i}{\partial p^c_j}$ then become

$$\frac{\partial(\beta_i - \theta_i)}{\partial p^c_j} = -\frac{1}{\cos\beta_i}\left(\frac{1}{R_i}\frac{\partial x_i}{\partial p^c_j} + x_i \frac{\partial(1/R_i)}{\partial p^c_j}\right) + \frac{1}{\cos\theta_i}\left(\frac{1}{R_i}\frac{\partial x_i^E}{\partial p^c_j} + x_i^E \frac{\partial(1/R_i)}{\partial p^c_j}\right). \qquad \text{(IV.8)}$$

By setting $\beta_i = \theta_i$ and $x_i = x_i^E$, good approximations for reflections near the Ewald sphere, we obtain

$$\frac{\partial\Delta\beta_i}{\partial p^c_j} = \frac{1}{R_i \cos\theta_i}\left(\frac{\partial x_i^E}{\partial p^c_j} - \frac{\partial x_i}{\partial p^c_j}\right). \qquad \text{(IV.9)}$$

It remains to evaluate $\partial x_i/\partial p^c_j$ from (II.1) and $\partial x_i^E/\partial p^c_j$, which can be done using the relation

$$x_i^E = -R_i^2 \lambda/2,$$

where the length R_i of reciprocal-lattice vector i has to be written as a function of unit-cell parameters.

The program written to implement this procedure accepts initial estimates of crystal orientation, unit cell and rocking curve parameters.* It computes improved values by the usual iterative least-squares procedure, applying shifts determined at each stage by solution of (IV.4). After each cycle of parameter refinement, data from the photograph in question are re-scaled to the reference set by equating the sum of intensities classified as fully recorded to the sum of their reference-set counterparts. Any of the parameters may be kept fixed.

As discussed in § II, the misorientation angles ε_x^t, ε_y^t, ε_z^t are defined at a particular setting t. As $\partial\beta/\partial\varepsilon_x = 0$, ε_x^t cannot be determined from partial spot information at one setting. To determine ε_x^t one needs such information at another setting, ideally differing by $\pi/2$ in the oscillation angle φ. In the one crystal–one photograph situation, the two settings differ by only a very small rotation of $\Delta\varphi$ around z. As a consequence, ε_x cannot be determined, and it is set to zero. For the determination of ε_y, partial spots at φ^b and φ^e are treated identically and φ^t in (II.1) is set to the mean oscillation angle φ^m. However, ε_z^b and ε_z^e are refined independently. Since the oscillation range $\Delta\varphi = (\varphi^b - \varphi^e)$ should, in principle, be known accurately from the camera setting, provision is made to adjust only φ_m, keeping $\Delta\varphi$ fixed.

The example of ε_x illustrates in an extreme way that the recorded fractions of reflections of one single photograph are not equally sensitive to all parameters considered in the refinement. Changes in some unit-cell

* The present version allows refinement of cell constants, of the misorientation angles ε_y, ε_z^b and ε_z^e, and of the rocking curve parameters γ_0 and γ_1 for either the step function or cosine-half-wave profile.

parameters or in certain linear combinations of them may also have no significant effect on the calculated fractions or, if they do, they may be highly correlated with a correction of one of the orientation parameters. In severe cases the refinement may not converge, especially if the starting point is far from the minimum. In such cases it is advisable to examine critically the correlation coefficients and the eigenvalue spectrum of the normal matrix. This will then indicate which parameter (or linear combination of parameters) should be held invariant.

The parameters being refined are sensitive only to the intensities of reflections that are actually *partially* recorded on the film. Only these reflections should therefore be included in the calculation. At any cycle, however, classification of reflections as fully recorded ($P_{cal} = 1$), partially recorded ($1 > P_{cal} > 0$) or not recorded ($P_{cal} = 0$) is subject to errors in the current values of the parameters. Refinement is therefore in practice complicated by some variation in the population of observations included from cycle to cycle. The farther one is from the minimum, the more reflections will be misclassified, slowing convergence. It is therefore useful to include at any cycle, in addition to reflections classified as partially recorded, those that would become so classified after small shifts in the values of the parameters. For the step function profile, the recorded fraction, P_{cal}, is proportional to the distance of a reciprocal lattice point from the Ewald sphere. If we do not restrict the value of $f(b)$ in (III.2) to the range 0 to 1, P_{cal} assumes values greater than 1 for fully recorded reflections and negative values for not recorded reflections. For example, in TBSV data collection, we included reflections with $-0{\cdot}2 < P < 1{\cdot}2$. We can also generalize a step-function profile to deal with the problem that reflections with $b_i < 0$ or $b_i > 1$ have undefined derivatives, $\partial f(b_i)/\partial p_j$, for a rocking curve of finite width. For the step function, $f(b_i) = b_i$, and meaningful derivatives are obtained even if b is not restricted to the range -1 to 1. Other profiles cannot simply be extended, but the derivatives for fully recorded and not recorded reflections to be included in the refinement can be calculated as if a step function profile were being used. By restricting P to the range 0 to 1 in the last cycle, it can be shown that this procedure improves convergence but does not in general bias the values of the parameters.

V. A practical case: TBSV 2·9 Å data collection

We illustrate the methods just outlined, by describing in detail the procedure of data collection from TBSV at 2·9 Å. Some steps in this work relied for convenience on the availability from earlier work of a complete 5·5 Å data set (Winkler, Schutt, Harrison & Bricogne, 1977), but this is by no means an essential feature. Successful completion of the structure determination at 2·9 Å has already been reported (Harrison *et al.*, 1978).

Data recording, densitometry, film pack scaling

The assessment of various sources of errors as well as the evaluation of the partial-spot correction procedure depends on realistic estimates of data precision. The following account shows how we obtained these estimates, pointing out precautions taken to minimize systematic errors in intensity measurements.

All photographs were taken on a Supper oscillation camera (Charles Supper Co., Natick, Mass.) at a crystal-to-film distance of 100 mm, using Cu $K\alpha$ radiation (Elliott GX6, 100 μm × 1 mm focus, 40 kV, 20 mA) focused by a double-mirror system of the Franks type (Harrison, 1968). A complete data set could be recorded on 50 photographs, each 25 to 35′ oscillation, covering a total contiguous arc of 25° around the [101] axis as indicated in Fig. 3. An important advantage of this particular choice is that the part of the crystal exposed to X-rays can be regarded as a plate parallel to the capillary wall, with its normal tilted by at most 25° with respect to the beam. This minimizes absorption effects. Since the beam diameter is smaller than the crystal, a significant change of the irradiated volume during oscillation must be avoided. This is guaranteed both by the very small oscillation range and by the morphology of the crystal and its relative orientation to the X-ray beam. Films were densitometered using a PDP-11/20-linked Optronics Photoscan (50 μm raster size) and a modified version of the program *SCAN*12 (Crawford, 1977).

Fig. 4 shows a photograph with about 20 000 reflections, of which 25–30% are fully recorded. Each photograph has a major zone axis almost perpendicular to it, permitting indexing of reflections by simple counting of lattice lines and lunes (layers). In this way eight reflections are indexed (two in each quadrant with one at each end point of the oscillation), visually judged to be partially recorded from their incomplete spot shapes. They are needed to determine the corrections ε_x

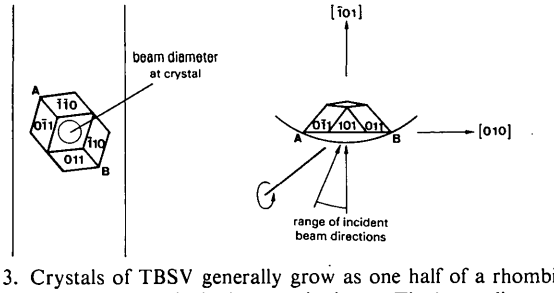

Fig. 3. Crystals of TBSV generally grow as one half of a rhombic dodecahedron. A typical alignment is shown. The beam diameter is about 0·1 mm at the crystal, the direction of the beam varies as indicated from 0 to 25°.

and ε_z (§ II and IV) that must be applied to the nominal setting of the crystal before densitometry. This preliminary crystal orientation refinement is similar to the one described in § IV and is needed for reliable prediction of reflections to appear on a photograph. A somewhat large value of 15′ was assumed for the reflecting range (2γ) in this calculation. The initial orientation of the film on the scanner was then found as follows: intensities of reflections predicted to be fully recorded and lying within the 5·5 Å resolution sphere were checked (off-line) in the available complete 5·5 Å data set and the strongest three in each quadrant selected. The scanner was programmed to locate the marked center of the film and then to find these twelve reference spots – easily achieved, since the pronounced lattice lines enable the film to be mounted with the direction of the spindle axis parallel within 1° to the horizontal scanner axis. Next the film-center coordinates and χ, the angle relating film and scanner coordinate systems, were refined. As ε_x is set to zero in the orientation refinement, the value of χ obtained in this refinement is the sum of the true χ, defined *e.g.* by fiducial marks on the film, and the true ε_x (for small ε_x, χ and ε_x are highly correlated). With some care in manual orientation of the crystal by still photographs, the error in ε_x can be kept smaller than 0·1°.*

Each film was scanned in three ranges ('annuli') starting at 6 Å resolution (Fig. 5). To allow a check that drift in the measured intensities did not occur during the few hours a film resided in the scanner, the ranges overlapped by about 100 reflections. In each annulus twelve strong, fully recorded reflections were located by a fast prescan, and new values of the parameters relating film and scanner coordinate systems were refined for each annulus. With the exception of the innermost annulus, the spot shape varies considerably with position on the film. To account for variability with angular position around the beam direction four different 'masks' were chosen, determining the sampling of spot intensity and background (Fig. 5, masks *A* to *D*). The close spacing of individual reflections dictated the choice of background positions; a sample rectangular box would have led to overlap of background points and adjacent spots. The size of the masks was chosen to be independent of distance from the film center, since the increase in size from 6 to 2·9 Å was not very large. A smaller rectangular box was used whenever reflections in the innermost annulus were measured. During densitometry, the intensity centroid of each spot was determined and, if necessary, the mask was shifted by up to two raster points along each scanner axis. The intensity centroid of reflections with a small recorded fraction may be displaced from the predicted center by more than this permitted limit, which is set by the close spacing of adjacent spots. In such cases the mask was set to the unshifted position.

For each reflection, the integrated intensity was output together with a standard deviation estimated from fluctuations in the spot background and from the average optical density of spot and background area (Arndt & Wonacott, 1977, p. 185). Measurements from the two films in each pack were scaled by the method of Fox & Holmes (1966). In this, as in all subsequent steps where multiple measurement were combined, a weighted mean was calculated, with weights given by the inverse variance carried along with each reflection. The variance of the weighted mean was obtained from the variances of the contributing measurements, unless there was a large discrepancy. In this case the variance was either increased or, in sets having several measurements, anomalous ones were

* This error must be kept small because of a significant effect on the Lorentz factor of reflections near the oscillation axis (*cf.* Arndt & Wonacott, 1977, p. 86).

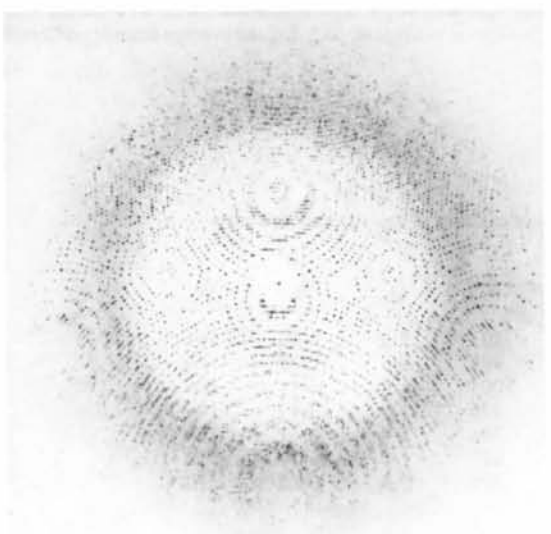

Fig. 4. Oscillation photograph (0·5°) of TBSV crystal; 17·5 h exposure.

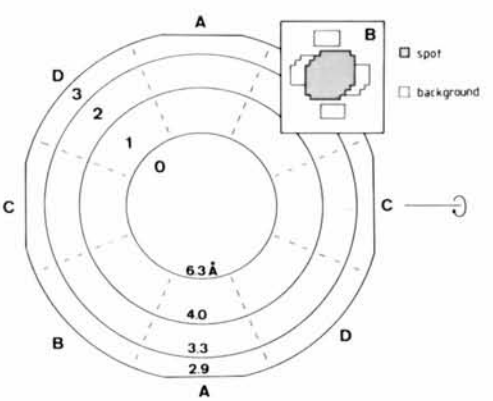

Fig. 5. Films were densitometered in four ranges. In the central area (0) a rectangular spot box was used; in annuli 1–3, four different masks (*A*–*D*) were used according to the angular position of the spot as indicated. As an example, mask *B* is shown.

rejected. Variances assigned during densitometry were corrected by a single factor to bring the estimated level of variation to that observed between measurements from different films in a pack. The updating of error estimates at each step of data processing where a large number of multple measurements are combined is useful for assessing the magnitude of various sources of errors that appear at different stages of data combination.

Evaluation of the partial spot correction procedure

Before routine processing of all photographs could be considered, it had to be established that the procedure outlined previously would give satisfactory results to the resolution limit. Eighteen of the fifty native photographs were selected for a detailed analysis, the first step of which was to form a reference data set. Due to the cubic symmetry of TBSV almost any combination of photographs leads to a partial data set of reflections that are uniformly distributed in reciprocal space. Twelve of the eighteen photographs were processed using the crystal orientation parameters obtained before densitometry. To avoid misclassification of partially-recorded as fully-recorded reflections, the values of γ_0 and γ_1 (III.5) used in this processing were chosen conservatively large. To combine reflections from different photographs (crystals) a relative scale factor and an exponential factor (temperature factor) accounting for the relative fall-off of intensity with resolution were determined for each crystal. This was done by generating Wilson-type plots of mean intensity against $(\sin\theta/\lambda)^2$ for each photograph and by fitting these plots optimally together. Combination of the *ca* 5000 fully recorded reflections on each of the twelve photographs yielded a reference data set with about 50 000 independent reflections (~25% complete); 6000 of these had been measured two or more times, and some statistical values derived from these multiple measurements are given in Table 1. To judge whether observed discrepancies were reasonable in terms of the error estimates of intensity measurements the quantity Q_I, defined below, was calculated:

$$Q_I = \frac{1}{N}\sum_{i=1}^{N} \Delta_i^2/\sigma^2(\Delta_i).$$

The sum is over all independent pairs of equivalent reflections, Δ_i being the difference between their intensities and $\sigma^2(\Delta_i)$ the sum of the variances of the two measurements. It can be seen that the error estimates are generally too small for larger intensities, but not by much. The average absolute difference between equivalent reflections ($\bar{\Delta}_I$) is fairly constant over the resolution range, indicating that reflections at high resolution have been measured with the same absolute precision as those at lower resolution.

To evaluate the rocking-curve model and the quality of calculated recorded fractions, the six remaining test photographs were used. Thus the reference data set is from a completely independent set of crystals. The fit

Table 1. *Intensity statistics in intensity and resolution ranges for the combination of fully recorded, equivalent reflections from* 12 *oscillation photographs of TBSV*

Relative scale and exponential factors were determined from Wilson-type plots as described in the text. Intensities are on an arbitrary scale, N is the number of independent pairs of equivalent reflections in each range, Q_I is defined in the text, and $\bar{\Delta}_I$ is the average intensity difference of these pairs. The R factor is defined as

$$R = \frac{\sum_h \sum_{j=1}^{N_h} |I_{hj} - \bar{I}_h|}{\sum_h N_h \bar{I}_h},$$

where the reflection, h, has been measured N_h times and $\bar{I}_h$ is the weighted mean of each set of equivalent reflections.

Intensity range	N	Q_I	R	Resolution range	N	Q_I	R	$\bar{\Delta}_I$
0–300	1839	1·0	0·60	6·00–4·73	2293	1·5	0·08	152
300–600	1106	1·1	0·20	4·73–4·12	999	1·5	0·08	196
600–900	724	1·4	0·13	4·12–3·74	1003	1·4	0·11	204
900–1200	515	1·6	0·09	3·74–3·47	776	1·2	0·13	196
1200–1500	354	1·7	0·07	3·47–3·26	761	1·1	0·21	220
1500–1800	263	1·7	0·06	3·26–3·10	657	1·0	0·30	212
1800–2100	175	1·8	0·05	3·10–2·90	309	0·8	0·32	178
2100–2400	134	2·4	0·06					
2400–2700	97	1·6	0·04					
2700–3000	64	2·6	0·05					
>3000	215	2·1	0·04					
Overall		1·3	0·11					

obtained with a set of parameter values was judged by calculating the following three quantities:

$$Q_P = \frac{1}{N}\sum_{i=1}^{N}\frac{(P^i_{\rm obs}-P^i_{\rm cal})^2}{\sigma^2(P_{\rm obs})} = \frac{1}{N}\sum_{i=1}^{N}(\Delta P^i)^2\, w_i, \quad \text{(V.1)}$$

$$\left.\begin{aligned}\overline{\Delta P} &= \sum_{i=1}^{N}\Delta P^i\, w_i \Big/ \sum_{i=1}^{N} w_i\\ \overline{|\Delta P|} &= \sum_{i=1}^{N}|\Delta P^i| w_i \Big/ \sum_{i=1}^{N} w_i\end{aligned}\right\}, \quad \text{(V.2)}$$

where

$$w_i = \frac{1}{\sigma^2(P_{\rm obs})}.$$

The weights w_i have been introduced to enhance the contribution of the more accurate observations, with low $\sigma^2(P^i_{\rm obs})$, to the averages $\overline{\Delta P}$ and $\overline{|\Delta P|}$. $\sigma^2(P^i_{\rm obs})$ is $\sigma^2(I^i_P/I^i_R)$, and the variance in the ratio of two random variables is approximated by (Hamilton, 1964)

$$\sigma^2(I^i_P/I^i_R) = [\sigma^2(I^i_P)\,\sigma^2(I^i_R) + \sigma^2(I^i_P)(I^i_R)^2 + \sigma^2(I^i_R)(I^i_P)^2]/(I^i_R)^4. \quad \text{(V.3)}$$

As this approximation is only reasonable when $\sigma(I^i_R) < I^i_R$, reflections with relatively inaccurate reference intensities are rejected in the refinement and in the subsequent statistical analysis. Each test photograph had around 1500 reflections in common with the reference data set, more than two thirds of which were partially recorded. The quantities given above were calculated separately for fully and partially recorded reflections in classes, determined by resolution, reference intensity, angular position on the film, calculated recorded fraction $P_{\rm cal}$, estimated accuracy of observed recorded fraction $\sigma(P_{\rm obs})$ *etc.* Given a perfect model, realistic error estimates and large enough samples, Q_p should be close to 1 and $\overline{\Delta P}$ close to 0 in all classes. Larger values of Q, and $\overline{\Delta P}$ far from zero indicate residual systematic errors. These may be due to a poor parametrization of the rocking curve but also may be due to systematic effects from absorption, bad scaling, *etc.* The latter causes can be identified by comparison of the corresponding figures for fully recorded reflections.

In a first run, the parameters ε_y, ε^b_z, ε^e_z, γ_0 and γ_1 were refined for each of the six test photographs, and the statistics described above produced. The cosine-half-wave profile was used, and the cell edge was taken to be 383.5 Å as in the 5·5 Å work. Only observations with $\sigma(P_{\rm obs})$ smaller than 0·25 were accepted, amounting to 700 to 800 observations for each photograph. This limit is set by two conflicting requirements. Inclusion of a large number of inaccurate observations is inefficient, but selection of only those with very low $\sigma(P_{\rm obs})$ biases the distribution of observations, since the average $\sigma(P_{\rm obs})$ increases with resolution. The results obtained in this first round of refinement showed that the relative decrease of data precision with resolution was too large to allow independent refinement of γ_0 and γ_1. This was apparent from their large correlation coefficient (>0·99) and from the fact that physically unreasonable values were obtained in four of the six cases. When only γ_0 was refined in five resolution ranges (with γ_1 set to zero), large fluctuations were observed from range to range although there was a clear overall increase. Its average slope was about three times that expected from the α_1, α_2 wavelength separation. For all further work γ_1 was set to this average value and no longer refined. The average value of Q_p was 2·2 for partially and 1·8 for fully recorded reflections. A correction in the cell edge was indicated by the observation that $\overline{\Delta P}$ deviated from zero in opposite senses when reflections were grouped into classes according to whether they appeared on the top or bottom half of the film and whether they occurred at φ^b or φ^e (refinement of unit-cell parameters was not yet programmed at that stage). Correcting the cell edge to 383·2 Å reduced Q_p to 1·6 for the partially recorded reflections, and no other deficiency of the simple rocking-curve model was obvious. Using the step-function profile rather than the cosine-half-wave resulted in a small but significant increase of 0·01 to 0·02 in $\overline{|\Delta P|}$. Except for a smaller value of γ_0, which is to be expected, the refined parameter values remained essentially invariant. Clearly the cosine-half-wave profile is to be preferred, although the average improvement is only a fraction of the average accuracy of the observations. These relatively large inherent errors make it difficult to diagnose further improvements in the rocking curve profile. There are indications that a Gaussian profile might give another small improvement, but it has not been tried in practice. One also expects the profile to become asymmetric for reflections at higher resolution because of unequal intensity of the $K\alpha_1$ and $K\alpha_2$ lines. However, the even larger errors at high resolution seem to mask systematic discrepancies due to deviations from a symmetric profile. Relative to the inherent errors no substantial improvement appears possible even by using more detailed many-parameter profiles, and the appealingly simple cosine-half-wave profile was used for all further work.

The results given in Tables 2 and 3 illustrate the following important points.

(1) The values of Q_p and Q^F_p given in rows *A* show that the overall fit is equally good for the classes of partially and fully recorded reflections. That higher values of Q_p are obtained for the very best observations (Q^*_p) is partly due to the tendency to underestimate errors associated with larger intensities and partly to the fact that only in this class do errors from over-simplification of the rocking-curve model become noticeable. It seems safe to say that these errors are smaller than 0·05, on the average.

Table 2. *Agreement factors, Q_p, and values of selected setting parameters of six text photographs*

Results for three different sets of parameters are shown (a = 383·2 Å and γ_1 = 0·0024 rad in all cases).

		Q_p	Q_p^*	Q_p^F	φ^m	$\Delta\varphi$	ω	γ_0	$\Delta(\Delta\varphi)$
(1)	*A*	1·6 (492)	4·2 (44)	1·6 (468)	−13·679	0·557	45·004	0·000724	+0·016
	B	1·7	4·3	1·6	−13·679	0·541	45·005	0·000686	
	C	10·6	81·0	1·6	−13·684	0·541	45·036	0·000800	
(2)	*A*	1·6 (762)	3·1 (80)	1·7 (327)	−16·184	0·479	45·003	0·000837	−0·021
	B	2·4	7·2	1·7	−16·185	0·500	45·006	0·000954	
	C	13·4	77·0	1·7	−16·182	0·500	44·967	0·000800	
(3)	*A*	1·8 (569)	4·9 (38)	1·5 (441)	−16·744	0·524	45·015	0·000775	+0·024
	B	2·1	6·8	1·5	−16·743	0·500	45·017	0·000708	
	C	9·9	92·0	1·4	−16·746	0·500	45·054	0·000800	
(4)	*A*	1·5 (471)	2·8 (44)	1·9 (454)	−17·268	0·529	45·020	0·000438	+0·029
	B	2·4	8·7	1·9	−17·273	0·500	45·021	0·000526	
	C	2·7	9·8	1·9	−17·271	0·500	45·017	0·000800	
(5)	*A*	1·7 (64)	3·7 (73)	2·1 (347)	−19·296	0·462	45·007	0·000577	−0·038
	B	3·7	11·7	2·2	−19·297	0·500	45·003	0·000787	
	C	13·5	75·0	2·1	−19·309	0·500	45·034	0·000800	
(6)	*A*	1·4 (589)	2·5 (47)	1·7 (267)	−20·262	0·479	44·974	0·000759	−0·021
	B	2·0	5·5	1·7	−20·264	0·500	44·975	0·000762	
	C	3·4	18·0	1·7	−20·250	0·500	44·979	0·000800	

(*A*) Full refinement of parameters ε_y, ε_z^b, ε_z^e and γ_0, using only observations with $\sigma(P_{obs}) < 0{\cdot}25$. The reference data set used to obtain the approximately 500 observed intensity ratios for each film was prepared as described in Table 1. Note that none of the six test photographs were included in the reference set. (*B*) Same as (*A*) but $\Delta\varphi = (\varepsilon_z^e - \varepsilon_z^b)$ set to the nominal oscillation range and held invariant. (*C*) Refinement based on observed intensity ratios was not performed and angular variables were obtained from the refinement before densitometry based on eight visually observed partially recorded reflections (the standard film-scanning procedure – *cf.* Arndt & Wonacott, 1977, p. 109). Oscillation range $\Delta\varphi$ as in (*B*), and γ_0 set to an average value of 0·0008 rad.

Symbols: $Q_p(Q_p^*, Q_p^F)$ as defined in (V.1). Q_p and Q_p^* are for partially recorded reflections only, and the * refers to the subset of observations with $\sigma(P_{obs}) < 0{\cdot}05$. Q_p^F is obtained from the fully recorded reflections for which $P_{cal} = 1$. φ^m, $\Delta\varphi$, ω and γ_0 as explained in the text (§§ II and III) and $\Delta(\Delta\varphi)$ is the deviation of the refined oscillation range from the nominal setting of the camera spindle. The number of observations is given in parentheses in row *A*.

Table 3. *Values of $|\overline{\Delta P}|$ for the six test photographs, with three sets of variables A, B and C as described in Table 2*

$|\overline{\Delta P}|$ (defined in V.2) is given in five ranges determined by $\sigma(P_{obs})$, the error estimate of each observation (defined in V.3).

Range of $\sigma(P_{obs})$		0·00–0·05	0·05–0·10	0·10–0·15	0·15–0·20	0·20–0·25
(1)	*A*	0·04	0·07	0·10	0·12	0·16
	B	0·04	0·08	0·11	0·12	0·15
	C	0·24	0·15	0·16	0·16	0·18
(2)	*A*	0·04	0·07	0·11	0·12	0·17
	B	0·04	0·08	0·12	0·18	0·23
	C	0·25	0·17	0·17	0·18	0·22
(3)	*A*	0·05	0·08	0·10	0·16	0·16
	B	0·06	0·09	0·11	0·16	0·16
	C	0·27	0·17	0·18	0·18	0·20
(4)	*A*	0·04	0·07	0·11	0·15	0·17
	B	0·07	0·09	0·10	0·14	0·17
	C	0·08	0·10	0·12	0·15	0·18
(5)	*A*	0·05	0·07	0·11	0·13	0·17
	B	0·06	0·11	0·14	0·17	0·22
	C	0·21	0·18	0·19	0·20	0·24
(6)	*A*	0·03	0·06	0·11	0·15	0·17
	B	0·05	0·08	0·12	0·17	0·19
	C	0·09	0·09	0·13	0·17	0·20

(2) The numbers listed in rows *B* correspond to the refinement in which the oscillation range $\Delta\varphi$ was fixed at the value set on the camera. Although the mechanical precision of the spindle was checked to be around 0·01°, deviations of up to 0·04° are observed for the refined values. Negative and positive deviations $\Delta(\Delta\varphi)$ occur, ruling out systematic imprecision of the camera. We have not investigated the effect further and cannot say how much is due to mechanical imprecision and how much results from compensation of various kinds of systematic errors in the data. The improvement on refinement of $\Delta\varphi$ is appreciable, especially for the best observations. As refinement of $\Delta\varphi$ cannot harm the data and also is a useful diagnostic tool, it is recommended in all cases.

(3) To demonstrate the need for a refinement of this type, based on measured intensities and a reference data set, the same quantities were calculated with the orientation parameters determined before densitometry (*i.e.* from visually determined, partially recorded reflections). For the half reflecting range, γ_0, a value of 0·008 rad was chosen and γ_1 was the same as in the other two cases. Again the effect shows up most dramatically in

Q_p^* (row *C* in Table 2) but also in the first column of Table 3. If only the last column of this table is consulted, one is tempted to doubt the necessity of the second refinement. Obviously in this class, the inherent errors in the intensity measurements dominate the additional errors from imprecise parameter values.

The routine processing procedure adopted after this evaluation was to refine ε_y, ε_z^b, ε_z^e and γ_0 for each photograph and to correct all reflections with $P_{cal} > 0{\cdot}5$ to their fully recorded equivalents. Partially recorded reflections are de-weighted relative to fully recorded ones by associating a constant error of 0·05 with each P_{cal}. Neglecting the first term in (V.3), the variance of the corrected intensity becomes

$$\sigma^2(I_p/P_{cal}) = [\sigma^2(I_p)P_{cal}^2 + (0{\cdot}05)^2 I_p^2]/P_{cal}^4. \quad \text{(V.4)}$$

Obviously the accuracy of corrected intensities decreases rapidly with decreasing P_{cal}, and the weight of measurements corrected by a small P_{cal} becomes negligible compared to that of the equivalent fully recorded measurement. For this reason reflections with $P_{cal} < 0{\cdot}5$ were discarded. The final statistics obtained when the data from all fifty photographs were combined were very similar to those given in Table 1, the overall *R* factor being 0·13. The value given by (V.4) is a reasonable estimate of the accuracy of partially recorded reflections, which correlate as well as whole spots when their appropriate corrected variance is considered.

VI. Concluding remarks

Under one crystal–one exposure conditions, partially recorded reflections from oscillation photographs must be discarded unless the fractions of intensity recorded for such reflections can be determined with sufficient accuracy. We have shown this to be possible in the case of TBSV data collection, where following the procedure described in this paper recorded fractions were calculated with an average accuracy estimated to be better than 0·05. In the final data processing, all reflections calculated to be more than half recorded were corrected in this way and included in the data set. This reduces significantly the loss in data collection efficiency that would otherwise be suffered in such situations.

Our procedure for correcting partially recorded reflections depends on the assignment of an observed recorded fraction to each partially recorded reflection that is fully recorded on the same or another photograph. The method thus relies on redundancy in the recorded data and requires a simple rocking curve profile to model the fractional build-up of the intensity of reflections during crystal rotation. Since redundancy is in any case needed with very large unit cells to improve the inherently low average signal-to-noise ratio, its requirement in this method does not lower the overall efficiency of data collection. By minimizing the sum of squared residuals between calculated and observed recorded fractions, the observations are used to optimize the values of the unit-cell parameters and of the crystal-setting and rocking-curve parameters of each photograph. Use of the recorded fractions, calculated with the refined parameter values, as correction factors in data processing is only justified if the overall agreement is considered satisfactory and if no significant improvement in the rocking-curve profile and its parametrization can be diagnosed. No such improvement of the simple cosine-half-wave profile was apparent in the case of TBSV data. We note that these films were recorded from crystals with extremely small mosaicity – sufficiently small that beam crossfire dominates the measured γ. The use of Franks-camera optics then insures a relatively small rocking-curve half-width (Harrison, 1968). Other experimental conditions may require modified treatment of the rocking curve – in particular variation of beam width with other variables such as angular position of a reflection on the film. We do not believe, however, that more detailed profile shapes are necessary with data of accuracy comparable to ours.

This work was supported by NIH Grant CA-13202 (to SCH). FKW acknowledges a fellowship from the Swiss National Fund, and SCH a PHS Research Career Development Award (CA-70169) and a Sloan Foundation Fellowship.

References

ALEXANDER, L. E. & SMITH, G. S. (1962). *Acta Cryst.* **15**, 983–1004.

ARNDT, U. W. & WONACOTT, A. J. (1977). *The Rotation Method in Crystallography*. Amsterdam: North-Holland.

CRAWFORD, J. (1977). PhD Thesis, Harvard Univ.

DIAMOND, R. (1969). *Acta Cryst.* A**25**, 43–55.

FOX, G. C. & HOLMES, K. C. (1966). *Acta Cryst.* **20**, 886–891.

GRANT, D. F. & GABE, E. J. (1978). *J. Appl. Cryst.* **11**, 114–120.

HAMILTON, W. C. (1964). *Statistics in Physical Science*, p. 33. New York: The Ronald Press Company.

HARRISON, S. C. (1968). *J. Appl. Cryst.* **1**, 84.

HARRISON, S. C., OLSON, A. J., SCHUTT, C. E., WINKLER, F. K. & BRICOGNE, G. (1978). *Nature (London)*, **276**, 368–373.

WINKLER, F. K., SCHUTT, C. E., HARRISON, S. C. & BRICOGNE, G. (1977). *Nature (London)*, **265**, 509–513.